

# UAL/ETEAPOT Proton EDM Benchmark Comparisons III: Dispersion, Longitudinal Dynamics and Synchrotron Oscillations

J. D. Talman and R. M. Talman

January 10, 2013

## Abstract

UAL/ETEAPOT is used to study longitudinal dynamics in the three benchmark lattices documented in Proton EDM Benchmark Comparisons I[1] and II[2]. These lattices have field indices  $m = -1$ ,  $m \approx 0$ , and  $m = 1$ . Most of the results this time are presented only for one or the other of the  $m = -1, 0, 1$  cases, since most longitudinal quantities are very nearly the same for all three once their vertical tunes have all been adjusted to  $Q_y=0.2$ .

The three benchmark lattices were chosen to be especially simple, with optics dominated by the (weak focusing) electric bend elements. Unfortunately the resulting extremely large dispersion complicates the longitudinal dynamics.

Evaluations of dispersion, synchrotron oscillations, and physical acceptances are compared with analytical calculations and with calculations using the same linearized transfer matrix formalism described in the earlier benchmark reports[1][2]. Agreement is excellent for the lattice dispersion, but ETEAPOT finds small-amplitude synchrotron tunes to be 15% greater than the analytic approximation predicts. This may be due to the neglect (in the analytic calculation) of the quadrupoles used to adjust the tunes to standard values. It may also be due to hyper-sensitivity resulting from the high lattice dispersion.

Accepting the ETEAPOT simulation results as valid, a detailed study of longitudinal motion is completed. There is excellent agreement with the expectations for  $Q_s$  to vary proportional to the square root of RF voltage and for the bunch length to vary approximately inversely to the square root of RF voltage. Stability for at least one million turns is demonstrated for sufficiently small synchrotron oscillation amplitude; any spurious growth in the simulation has a growth lifetime of at least three million turns. Both qualitatively and quantitatively synchrotron oscillations seem to behave in electric lattices much the way they do in magnetic lattices.

But a novel growth phenomenon is observed in which particles of intermediate amplitude (small enough to remain inside the physical aperture for at least several synchrotron oscillation periods) can grow and wipe out on longer time scales. If confirmed this implies the horizontal dynamic aperture of weak focusing proton EDM rings will be substantially smaller than their physical aperture would superficially indicate.

January 3, 2013

# 1 Parameters of Benchmark Lattices

Transverse parameters for the benchmark lattices are given in Table 1; these have been copied from previous reports. Longitudinal parameters of the same lattices are given in Table 2; the entries are explained in later sections.

Table 1: Transverse parameters of benchmark all-electric EDM lattices copied from benchmark comparisons I[1] and II[2].

file name	variable name	unit	E_BM_M1.0.RF.sxf	E_BM_Z.RF.sxf	E_BM_P1.0.RF.sxf
cells/arc	NCellPerArc		20	20	20
bend radius	r0	m	40.0	40.0	40.0
half drift length	Ldh	m	1.0	1.0	1.0
half bend per cell	Thetah	r	0.078539816	0.078539816	0.078539816
half bend length	Leh	m	3.141592	3.141592	3.141592
circumference	circum	m	331.327	331.327	331.327
inverse focal length	q	1/m	-0.002019	-0.00005960	0.0019075
field index	m		-1.0	1.0e-10	1.0
horizontal beta	betax	m	35.9237	36.1018	36.1910
vertical beta	betay	m	264.182	263.620	262.237
horizontal tune	Qx		1.4605	1.4578	1.4588
vertical tune	Qy		0.20024	0.20004	0.20047

Table 2: Longitudinal parameters (in MAD/UAL units) for the E\_BM\_M1.0.RF.sxf benchmark all-electric EDM lattice. Most of these quantities are very nearly the same for the E\_BM\_Z.RF.sxf and E\_BM\_P1.0.RF.sxf. This can be seen, for example, in Figure 3. Uncertainties in the analytic values are discussed in the text.

file name	symbol	unit	analytic	linearized model	ETEAPOT
Rev. period	$T_{\text{rev}}(\gamma_0)$	$\mu\text{s}$	1.846972	1.846972	1.846972
	$dT_{\text{rev}}/d\gamma _{\gamma_0}$	$\mu\text{s}$	2.49127		
RF frequency	$f_{\text{RF}}$	MHz	$0.541426 h_{\text{RF}}$		$0.541426 h_{\text{RF}}$
harmonic number	$h_{\text{RF}}$		100		100
RF peak voltage§	$\hat{V}_{\text{RF}}$	kV	1.0		1.0
RF phase lag¶	$\phi_{\text{RF}}$	radian	0.5		0.5
dispersion	$D_{\text{UAL}}$	m	66.9, Eq.(12)	$24.8 \times 2.74 = 67.9$	66.9, Fig.9
slip factor	$\eta_{\text{RF}}$		$\approx -0.92$ , Eq.(18)		0.0071, Fig.6
synch. tune (lo)	$Q_s(10^{-6})$		$\approx 0.0061$ , Eq.(19)		0.0066, Fig.11
synch. tune (hi)	$Q_s(2 \times 10^{-5})$				
ang. accept. (short)					$\pm 0.0004$ , Fig.10
ang. accept. (long)					$< \pm 0.0002$ , Fig.12

In SXF file: §RF voltage drop in GV, ¶RF phase shift in units of  $2\pi$

## 2 Definitions of Fractional Momentum or Energy Offset

Different communities prefer different definitions of the fractional momentum or energy offset. Wollnik (Section 4.1.1.2) defines the “rigidity offset”  $\Delta$  of an off-energy particle by

$$r = r_0(1 + \Delta), \quad \text{or} \quad \delta_{\text{Wollnik}} \equiv \Delta = \frac{r - r_0}{r_0}, \quad (1)$$

where  $r_0$  is the nominal bend radius, and  $r$  is the radius of a concentric circular orbit followed by the off-momentum particle. This is the fractional offset coordinate applicable to the linearized transfer matrix benchmark comparison results in this report. For “sector bends” in which all orbits enter and exit more or less normal to the edges of the bend element there is hardly any need to distinguish between radial offsets outside and inside bend elements.

UAL/ETEAPOT (like MAD) defines a fractional energy offset,

$$\delta_{\text{UAL}} \equiv \frac{\mathcal{E}^O - \mathcal{E}_0^O}{p_0^O c}. \quad (2)$$

The superscript  $O$  is attached to  $\mathcal{E}^O$  and  $p^O$  here to specify that these quantities are restricted to regions “outside” bend regions; i.e. where the potential energy vanishes. (For  $\mathcal{E}$  this notation is redundant since  $\mathcal{E}$  is preserved except in RF cavities. As it happens it is also redundant for  $p_0$  since, by definition, the potential energy vanishes everywhere on the design orbit.)

- It is shown in the UAL/ETEAPOT manual that the Wollnik  $\Delta$  parameter is related to the MAD/UAL momentum deviation factor  $\delta_{\text{UAL}}$  by

$$\Delta = \left(1 + \frac{1}{\gamma_0^2}\right) \frac{1}{\beta_0} \delta_{\text{UAL}} \quad (= 2.744 \delta_{\text{UAL}} \quad \text{for the proton EDM experiment.}) \quad (3)$$

- A notation commonly employed in the electron and proton accelerator worlds (with jargon “delta p over p”) is

$$\delta_p \equiv \frac{p^O - p_0}{p_0}. \quad (4)$$

(We intentionally refrain from introducing a momentum-inside variable  $\delta_{p^I}$ ; defined in terms of this variable the dispersion  $D_{\delta_{p^I}}$  would be singular for field index  $m = 0$ .) Relations among fractional *outside* momentum or energy coordinates, since they are unaffected by potential energy, can be obtained using standard (for magnetic lattices) kinematic formulas, starting from

$$\mathcal{E}^2 = p^2 c^2 + m_p^2 c^4. \quad (5)$$

For example,

$$\frac{dp}{p_0} = \frac{1}{\beta_0} \frac{d\mathcal{E}^O}{p_0 c}, \quad \text{or} \quad \delta_p = \frac{1}{\beta_0} \delta_{\text{UAL}}. \quad (6)$$

To obtain  $\delta_p$  (also known as “delta p over p”) from  $\delta_{\text{UAL}}$  one must therefore divide  $\delta_{\text{UAL}}$  by 0.6.

- Should one want the absolute change in  $\gamma$  corresponding to  $\delta_{\text{UAL}}$  one has to multiply  $\delta_{\text{UAL}}$  by  $p_0 c / (m_p c^2) = 0.7 / 0.938 = 0.746$ . This relation can also be expressed as  $d\gamma = \beta_0 \gamma_0 \delta_{\text{UAL}}$ .

Having established the principle behind the  $O$ -superscript notation, from here on quantities without superscripts are to be interpreted as *outside* quantities. This simplifies the discussion of synchrotron oscillations where it is assumed that the bend field electric potential vanishes throughout RF cavities.

### 3 Analytic Estimates of Longitudinal Parameters

This section discusses the analytical treatment used to estimate parameters for checking the numerical ETEAPOT results. It is the only section in which it is necessary to deal with the confusing subject of kinematic quantities in the interior of bend elements. The (weak) quadrupoles present in the lattice to trim the tunes are neglected for this treatment. This causes an uncontrolled, but hopefully small, uncertainty in the comparison values.

#### 3.1 Qualitative Discussion of Dispersion

For circular orbits in an electric bend element with radial electric field  $-E_0$ , the radius of the central orbit is given by

$$r_0 = \frac{m_p c^2 / e}{E_0} \gamma_0 \beta_0^2. \quad (7)$$

For field index  $m$  the radius of curvature of an off-momentum circular orbit is given by

$$r = r_0 \left( \frac{\gamma_0^2 - 1}{\gamma_0} \frac{\gamma^I}{\gamma^{I^2} - 1} \right)^{1/m}, \quad (8)$$

where  $\gamma_0$  is the value on the central orbit. This relationship is singular for field index  $m = 0$  (which is also known as the “cylindrical” case because the electrodes giving this radial dependence are cylindrical).  $m = 0$  is also the unique case in which the dependence of electric potential on radius  $r$  is logarithmic and cannot be expressed by a power law.

For values of  $m$  near 1 the orbit velocities of off-energy circular orbits within bend elements are approximately independent of  $r$ . This causes the time of flight of off-energy closed orbits through arcs (which are perfect circles) to be dominated by the arc length, which is the bend angle multiplied by  $r$ . Since the speed depends only weakly on momentum this is “above transition” behavior. On the other hand, off-energy closed orbit path lengths through drifts are independent of  $\delta_{\text{UAL}}$ , which causes time of flight of off-energy closed orbits through drifts to be dominated by the particle speed; this is “below transition” behavior. Assuming the drift lengths are fairly short, the net behavior is “above-transition” like.

For negative  $m$  values the radius of the off-energy closed orbit increases with increasing energy offset. The dispersion  $D$  is therefore positive for  $m < 0$ ; furthermore the magnitude  $|D|$  increases as  $m$  approaches zero. For positive  $m$  values (such as the  $m = 1$  “spherical case”) the radius of off-energy closed orbits decrease with increasing energy offset. The dispersion  $D$  is therefore negative for  $m > 0$ ; but the magnitude  $|D|$  again increases as  $m$  approaches zero.

Realistic lattices also have quadrupoles which affect the dispersion. But, since the quadrupoles are very weak in the three benchmark lattices, their influence on lattice dispersion can be expected to be not very important. (For the minimized-dispersion, strong horizontal focusing, combined function lattices to be recommended as a response to results in the present report, this will no longer be even approximately valid.)

Combining all these statements, the dispersion function  $D$  has to have a singularity in the vicinity of  $m = 0$ . It is the longitudinal dynamics (rather than the transverse) that is sensitive to lattice dispersion. To make them as simple as possible, the  $m$ -values of the three benchmark lattices were chosen close to zero. Inadvertently this choice has caused the longitudinal dynamics of the benchmark lattices to be hyper-sensitive.

An example of this hypersensitivity comes about in comparing computer simulation and analytic results. The analytic results depend on the dispersion. But the dispersion is not used, and is not available, during particle tracking. This makes it a priori unknown what RF phase will give stable longitudinal motion in simulation. We resolve this ambiguity by trying two RF phases differing by  $\pi$  and choosing the phase that gives stable motion.

Another subtle complication of operation near  $m = 0$  comes about because a particle having positive velocity offset outside bends can have either positive or negative velocity offset inside bends, depending

on the sign of  $m$ . This dependence is transparent to the computer simulation but complicates the analytic calculation of the “slip factor” needed to calculate the synchrotron oscillation frequency.

In a truly uniform, weak-focusing, electric ring the off-momentum closed orbits are true circles with radius  $r$ , in which case Eq. (8) provides an analytic formula valid for all amplitudes. For our purposes this is somewhat academic however, as explicit quadrupoles make the benchmark lattices slightly “separated-function”. Deflections in the quadrupoles cause the off-momentum trajectories to be somewhat non-circular in the bends.

### 3.2 Dispersion of the Benchmark Lattices

Of the benchmark lattices, the closest to the ideal case is the **E\_BM\_Z.RF** lattice for which the quadrupoles are very weak. We have found however, after the quadrupoles have been adjusted to give identical tunes for the three benchmark cases, that the longitudinal behaviors of the three lattices are essentially identical. For example we will use Eq. (8) to estimate the dispersion for the **E\_BM\_M1.0** lattice.

In Eq. (8) the value  $m = 0$  is singular; this corresponds to the fact that, for  $m = 0$ ,  $\gamma^I$  is equal to  $\gamma_0$ , independent of  $r$ . Exploiting this independence, and neglecting a small  $m$ -dependent term that comes from treating the radial electric field as being independent of  $r$ , the dependence of  $\gamma$  (which, remember, is  $\gamma^O$  by definition) and  $r$  is

$$\mathcal{E}^O = m_p c^2 \gamma \approx m_p c^2 \gamma_0 + e E_0 (r - r_0). \quad (9)$$

Differentiating with respect to  $r$  gives

$$d\mathcal{E}^O = e E_0 dr. \quad (10)$$

Using Eq. (2), this can be re-expressed as

$$dr = \frac{p_0 c / e}{E_0} \delta_{\text{UAL}}. \quad (11)$$

The UAL-units dispersion is therefore given by

$$r_{\text{co}}(\delta_{\text{UAL}}) = D_{\text{UAL}} \delta_{\text{UAL}}, \quad \text{where} \quad D_{\text{UAL}} = \frac{p_0 c / e}{E_0} = \frac{0.701}{10.48 \times 10^{-3}} = 66.9 \text{ m}. \quad (12)$$

Figures 8 and 9 obtained by UAL/ETEAPOT tracking, agree very well with this estimate. Especially Figure 9, for which horizontal betatron motion has been largely eliminated, the straight line fit using Eq. (12) agrees perfectly with the tracking results.

### 3.3 Slip Factor and Synchrotron Tune

The revolution period of the central particle is given by

$$T_{\text{rev}}(\gamma_0) = \frac{2\pi r_0 + D_{\text{tot}}}{\beta_0 c}, \quad (13)$$

where  $D_{\text{tot}} = 331.3274 - 2\pi \times 40 = 80.0 \text{ m}$  is the accumulated straight section length. Neglecting the effect of the quadrupoles, for an off-momentum closed orbit, the revolution period is

$$T_{\text{rev}}(\gamma) = \frac{2\pi r}{\beta_0 c} + \frac{D_{\text{tot}}}{\beta^O c}. \quad (14)$$

The constancy of  $\beta$  within the bend region in the  $m = 0$  case is exploited in the first term, but the actual  $\beta^O$  value has to be used in the second term. (Because  $D_{\text{tot}}$  is so short for the benchmark lattices, this term is small for the benchmark lattices. But for long straight sections, as in the FNAL option, time of flight through straight regions strongly influences the longitudinal motion.)

From  $\beta^2 = 1 - 1/\gamma^2$  we have, evaluated at  $\beta = \beta_0$ ,  $d\beta = d\gamma/(\beta_0 \gamma_0^3)$ . Using this in Eq. (9), and applying Eq. (12), the off-momentum, outside, velocity is

$$\beta^O \approx \beta_0 \left( 1 + \frac{1}{\beta_0^2 \gamma_0^3} \frac{E_0}{m_p c^2 / e} D_{\text{UAL}} \delta_{\text{UAL}} \right) = \beta_0 \left( 1 + \frac{D_{\text{UAL}} \delta_{\text{UAL}}}{r_0 \gamma_0^2} \right) \quad (15)$$

Substituting  $r - r_0 \approx D_{\text{UAL}}\delta_{\text{UAL}}$  also into Eq. (14) yields

$$\frac{T_{\text{rev}}(\gamma) - T_{\text{rev}}(\gamma_0)}{T_{\text{rev}}(\gamma_0)} = \frac{1}{C} \left( 2\pi \mp \frac{1}{\gamma_0^2} \frac{D_{\text{tot}}}{r_0} \right) D_{\text{UAL}}\delta_{\text{UAL}}, \quad (16)$$

where  $C$  is the circumference of the design orbit. The  $\mp$  factor in the second term allows for the fact that  $D_{\text{UAL}}$  can have either sign, while the phase slip in the straight section is necessarily negative. Edwards and Syphers[3] define the “slip factor”  $\eta_{\text{RF}}$  by

$$\frac{T_{\text{rev}}(\gamma + \Delta\gamma) - T_{\text{rev}}(\gamma_0)}{T_{\text{rev}}(\gamma_0)} = \frac{\eta_{\text{RF}}}{\beta_0^2} \frac{\Delta\gamma}{\gamma_0}, \quad (17)$$

and we obtain

$$\eta_{\text{RF}} = \beta_0 \left( 2\pi \mp \frac{1}{\gamma_0^2} \frac{D_{\text{tot}}}{r_0} \right) \frac{D_{\text{UAL}}}{C} = -0.92. \quad (18)$$

As mentioned above, the negative sign is accounted for in the tracking simulation by shifting the RF phase appropriately to produce stable motion.

Edwards and Syphers give the synchrotron tune in terms of the slip factor:

$$Q_s = \sqrt{\frac{1}{2\pi} \frac{h_{\text{RF}}\eta_{\text{RF}} \cos(2\pi\text{lag})}{\beta_0^2\gamma_0} \frac{V_{\text{RF}}}{m_p c^2/e}} = 0.0061. \quad (19)$$

The  $\eta_{\text{RF}} \cos(2\pi\text{lag})$  product needs to be positive for the synchrotron oscillations to be stable. The lag factor, which establishes the RF phase, is read in from the SXF lattice description file. (This is discussed further in a concluding section.)

## 4 Determination of Dispersion Function from Transfer Matrices

Orbit evolution from the origin at  $s = 0$  to a general position  $s$  can be expressed by a transfer matrix  $\mathbf{M}(s, 0)$ :

$$\begin{pmatrix} x(s) \\ x'(s) \\ \delta \end{pmatrix} = \begin{pmatrix} M_{11}(s, 0) & M_{12}(s, 0) & M_{13}(s, 0) \\ M_{21}(s, 0) & M_{22}(s, 0) & M_{23}(s, 0) \\ 0 & 0 & 1 \end{pmatrix} \begin{pmatrix} x(0) \\ x'(0) \\ \delta \end{pmatrix}. \quad (20)$$

Note that the third component is conserved except at RF cavities. Also some of the matrix elements depend on the definition of  $\delta$ . After associating a transfer matrix to each of the elements in the ring,  $\mathbf{M}(s, 0)$  is found by “concatenating” (i.e. multiplying) these matrices.

For fully-relativistic magnetic lattices the third component  $\delta$  is customarily referred to as  $\delta p/p$ , and this coordinate can be identified almost exactly with  $\delta\gamma/\gamma$  or with fractional energy offset (from the design orbit). But for an only weakly-relativistic EDM lattice which, furthermore, has electric bending, it is necessary to be more careful. For now we leave the definition of  $\delta$  open, planning to replace it by one or the other of the fractional offset coordinates introduced in the previous section. Of course the dispersion function  $D_\delta(s)$  becomes definite only when  $\delta$  is defined unambiguously.

The “off-momentum closed orbit”  $x_{\text{c.o.}}(\delta, s)$  is defined to be the unique orbit which, for longitudinal phase space displacement  $\delta$ , closes on itself after a complete turn around the ring. The dispersion is then defined, in linearized approximation, by

$$x_{\text{c.o.}}(\delta, s) = D_\delta(s) \delta. \quad (21)$$

Since the transfer matrix includes a description of the influence of energy offset, it can also be used to find the dispersion function  $D_\delta(s)$ . First the “fixed point” at the origin,  $(D_\delta(0), D'_\delta(0))$  has to be found. If the lattice has mirror symmetry, which is true for the benchmark lattices, the origin can be chosen on the axis of symmetry, and  $D(s)$  is also mirror-symmetric; in this case  $D'(s)|_{s=0} = 0$ .

Evolution once around the ring, starting from the origin, of an off-energy particle on the closed orbit corresponding to its energy is described by the “once-around” transfer matrix  $\mathbf{M}$ :

$$\begin{pmatrix} D(0) \delta \\ 0 \\ \delta \end{pmatrix} = \begin{pmatrix} M_{11} & M_{12} & M_{13} \\ M_{21} & M_{22} & M_{23} \\ 0 & 0 & 1 \end{pmatrix} \begin{pmatrix} D(0) \delta \\ 0 \\ \delta \end{pmatrix}. \quad (22)$$

This provides two formulas,

$$D(0) = \frac{M_{13}}{1 - M_{11}} = -\frac{M_{23}}{M_{21}}, \quad (23)$$

one of which can be used as a consistency check. Evolution around the ring of  $D(s)$  and  $D'(s)$  is then given by

$$\begin{pmatrix} D(s) \\ D'(s) \\ 1 \end{pmatrix} = \begin{pmatrix} M_{11}(s) & M_{12}(s) & M_{13}(s) \\ M_{21}(s) & M_{22}(s) & M_{23}(s) \\ 0 & 0 & 1 \end{pmatrix} \begin{pmatrix} D(0) \\ 0 \\ 1 \end{pmatrix}. \quad (24)$$

Spelled out explicitly,

$$\begin{aligned} D(s) &= D(0) M_{11}(s) + M_{13}(s), \\ D'(s) &= D(0) M_{21}(s) + M_{23}(s). \end{aligned} \quad (25)$$

## 5 ETEAPOT Longitudinal Dynamics Plots

Figure 1 shows the evolution, for 20,000 turns, of the four horizontal phase space degrees of freedom of a single particle with starting coordinates  $(x, x', ct, \delta_{UAL}) = (0, 0, 0, 0.000001)$ . The initial populated 4-volume starts from zero but jumps almost immediately to the finite (but large) 4-volume shown. Subsequent graphs are intended to investigate finer features of this evolution.

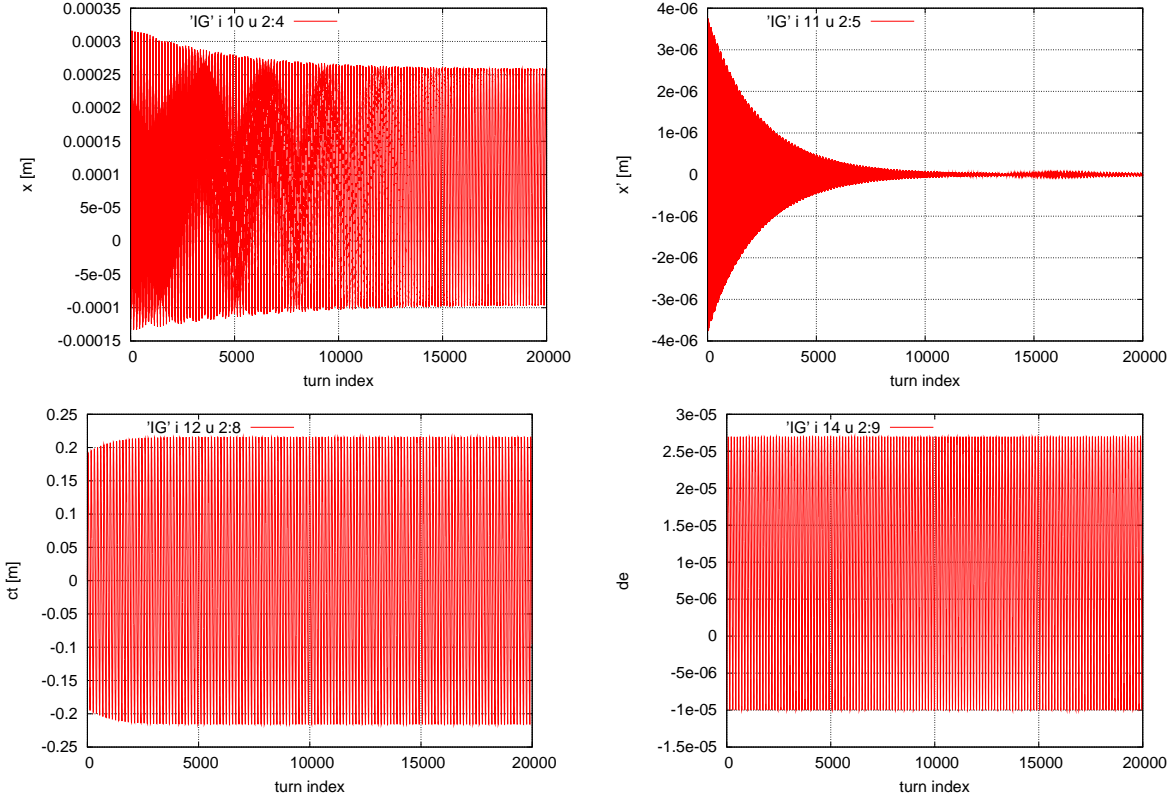


Figure 1: Starting from  $(x, x', ct, \delta_{UAL}) = (0, 0, 0, 0.000001)$  a single particle with initial energy displacement  $\delta_{UAL} = 0.000001$  (or  $de=0.000001$ ) visits the regions of horizontal phase space shown during 20000 turns. The upper two plots are “horizontal betatron space”, the lower two are “longitudinal space”.

Longitudinal dynamics in lattice `BM_M1.0.RF` (having  $m=-1$ ) is shown in Figure 2. (For the outermost amplitude the initial conditions have been adjusted to eliminate the initial betatron amplitudes.) The three benchmark lattices are compared in the similar plots of Figure 3. For this comparison only the three innermost amplitudes are tracked. In these plots three particles start at the origin traveling in the forward direction, with fractional energy offsets  $\delta_{UAL} = 0.000001, 0.000002, 0.000003$ . The three plots are essentially identical. We interpret this to mean that the quadrupoles adjacent to the bend elements, having been adjusted to restore the vertical tune to its standard value  $Q_y = 0.2$ , effectively cancel the focusing effect coming from non-zero field index  $m$ . In other words, as far as longitudinal dynamics is concerned, the three benchmark lattices are equivalent.

Fractional offset  $\delta_{UAL} \equiv \delta\mathcal{E}/(p_0c)$  is plotted against turn number for a range of values of RF amplitude  $\hat{V}_{RF}$  in Figure 4. The corresponding longitudinal phase space plots are shown in Figure 5.

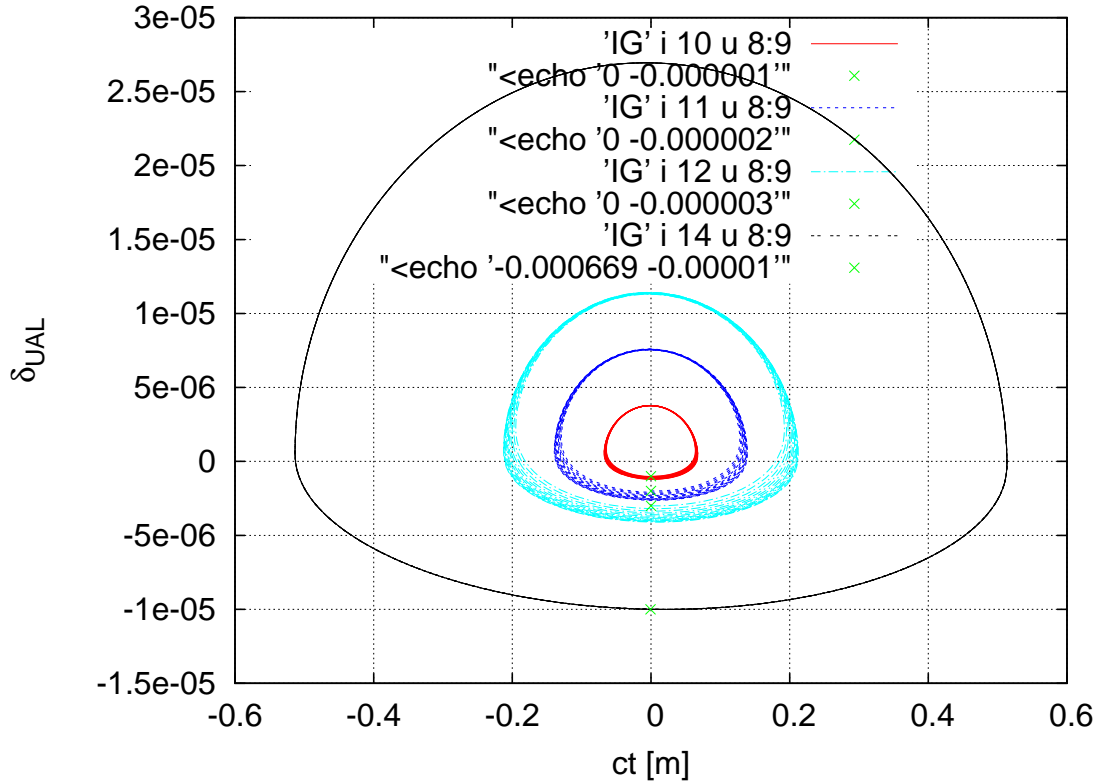


Figure 2: The longitudinal phase space for the `BM_M1.0.RF` lattice is extended to large amplitudes approaching the limit of stability for the given RF parameters. Fractional energy offsets are  $\delta_{UAL} = 0.000001, 0.000002, 0.000003, 0.000010$ . Unlike the inner three contours, for the outermost contour the particle was launched with negligible initial betatron amplitude.

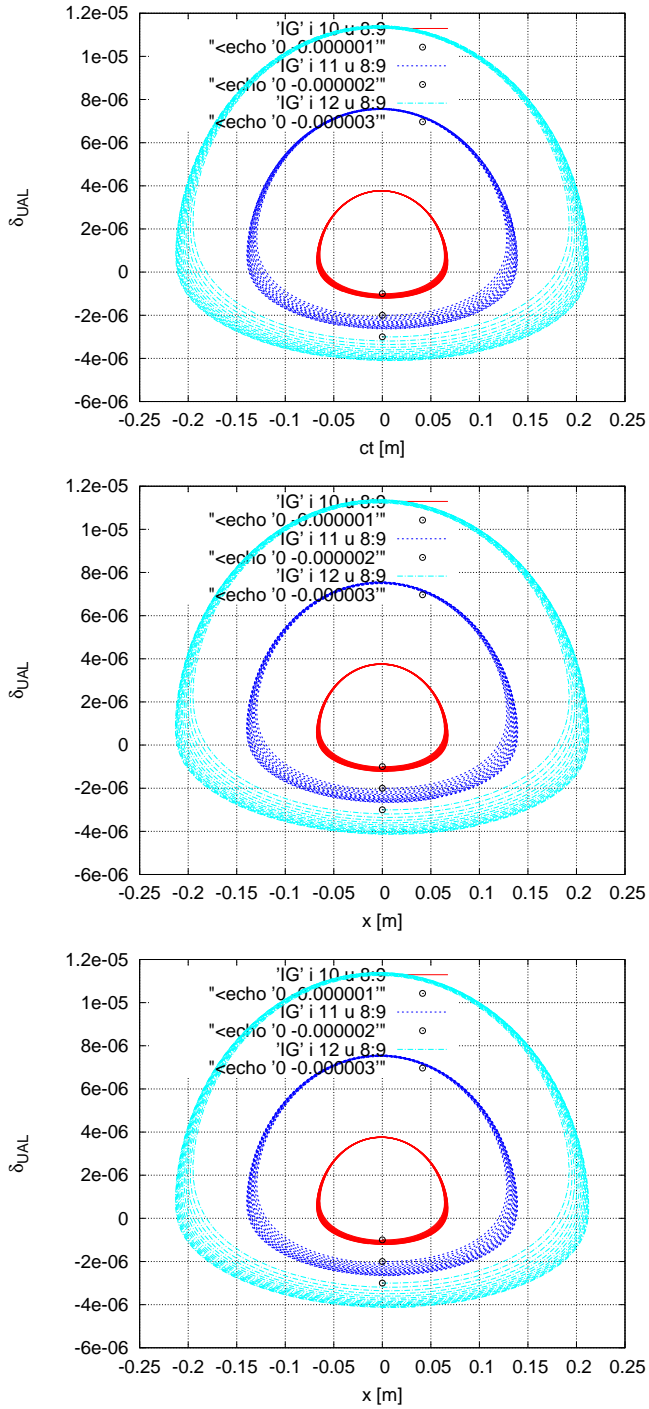


Figure 3: Longitudinal phase space plots for lattices (from top to bottom) BM\_M1.0.RF, BM\_Z.RF, and BM\_P1.0.RF.

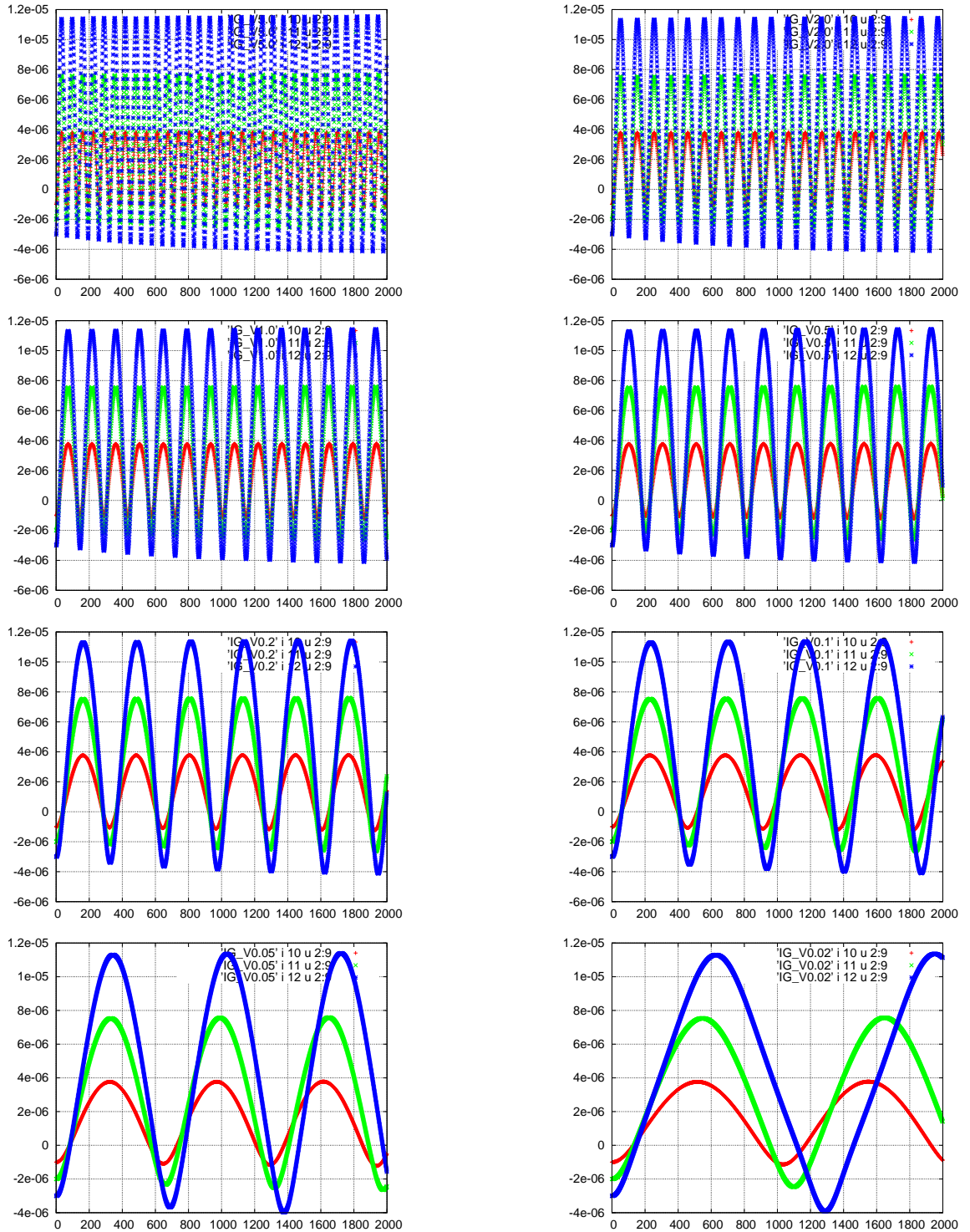


Figure 4: Fractional offset  $\delta_{UAL} \equiv \delta\mathcal{E}/(p_0c)$  plotted against turn number for values of RF amplitude  $\tilde{V}_{RF}$  5.0, 2.0, 1.0, 0.5, 0.2, 0.1, 0.05, 0.02 [kV]—reading from left to right then top to bottom; lattice BM\_M1.0.RF. Each of the plots shows three synchrotron oscillation amplitudes. Starting from the origin with vanishing slopes, the initial “momentum offsets” are  $\delta_{UAL}=-0.000001$ ,  $-0.000002$ , and  $-0.000003$ . Extending the third graph to  $10^5$  and then  $10^6$  turns showed no growth nor decay nor any noticeable change whatsoever. A figure “delta\_vs\_turn\_Z.RF\_sl4.eps” (not shown) has four-times finer slicing and is also essentially indistinguishable from the third graph ( $V_{RF}=1$  kV).

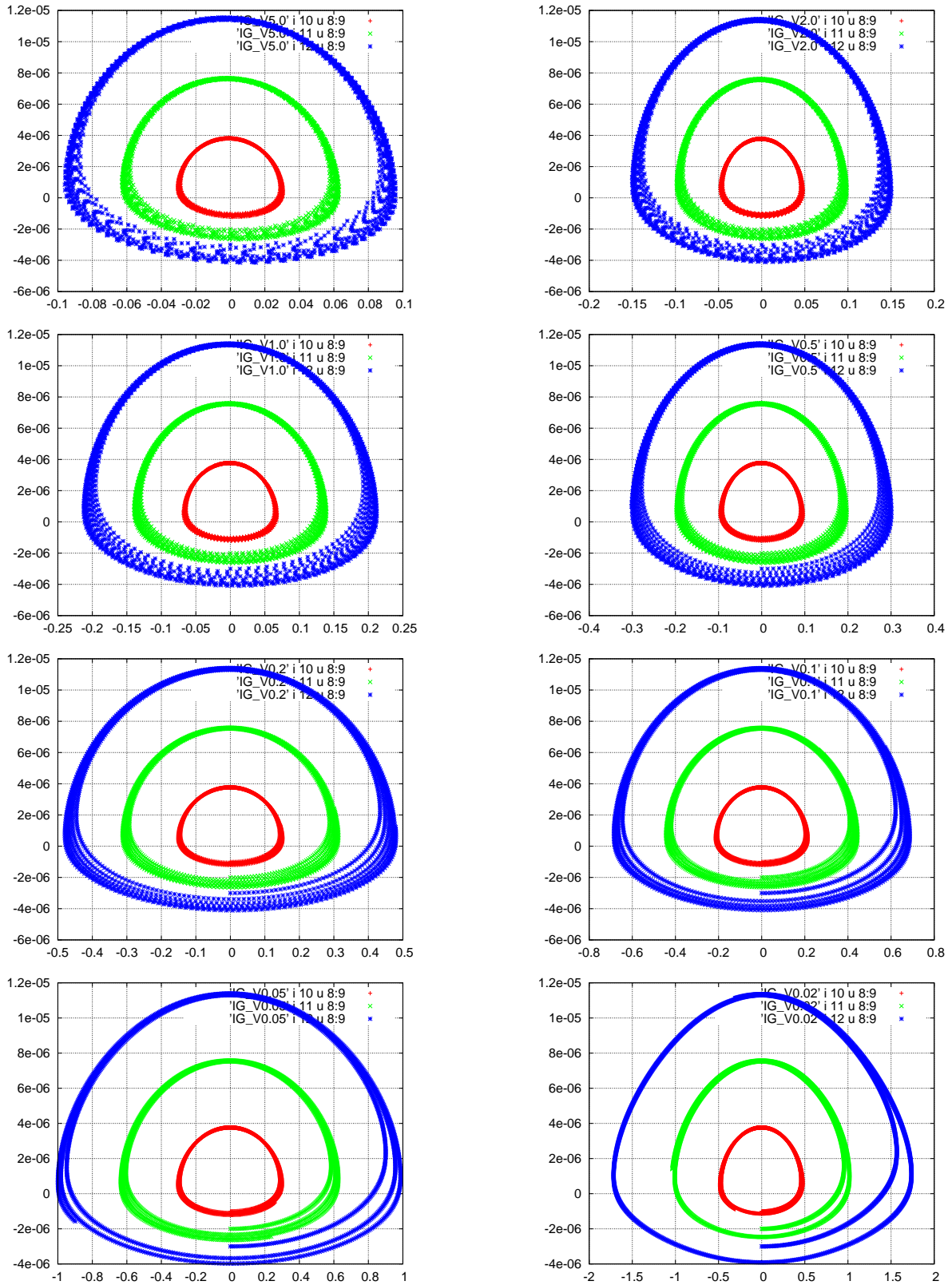


Figure 5: Longitudinal phase space plots for the same series of RF voltages, 5.0, 2.0, 1.0, 0.5, 0.2, 0.1, 0.05, 0.02 [kV] as in Figure 4.

From Figures 4 and 5 data can be extracted to produce Figure 6 and Figure 7 which plot the synchrotron tune  $Q_s$  and the bunch length  $\ell_B$  as functions of  $V_{RF}$ . Fitting functions are shown in the captions to the figures. The strict proportionality  $Q_s \sim \sqrt{V_{RF}}$  is consistent with Eqs. (19). In the approximately linear region of the plot  $\ell_B$  is proportional to  $1/\sqrt{V_{RF}}$ .

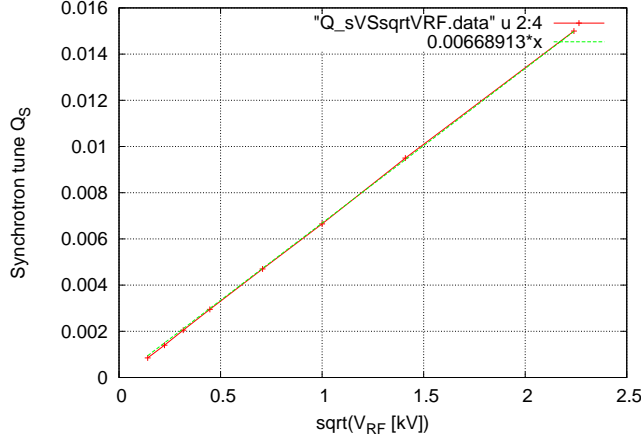


Figure 6: Plot of synchrotron tune  $Q_s$  (obtained by counting periods in plots like those in Figure 4) versus  $\sqrt{V_{RF} [\text{kV}]}$ . (This plot was actually obtained from an earlier, but almost identical series of graphs.) The fit yields  $Q_s = 0.00669\sqrt{V_{RF} [\text{kV}]}$ .

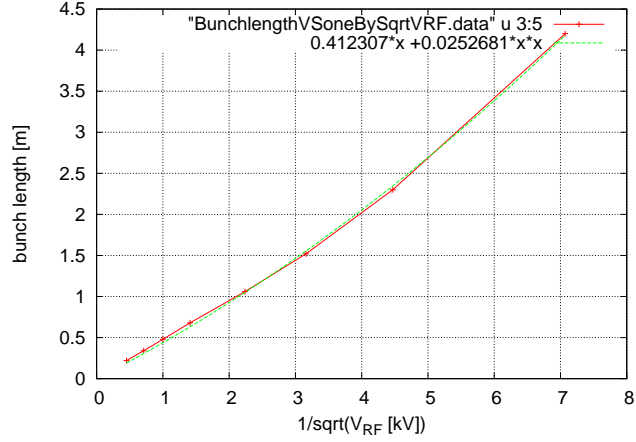


Figure 7: Plot of bunch length (extremes in plots like those in Figure 5 for  $\delta_{UAL}=0.000003$ ) versus  $1/\sqrt{V_{RF} [\text{kV}]}$ . (This plot was actually obtained from an earlier, but almost identical series of graphs.) The fit yields  $l_B = 0.4123/\sqrt{V_{RF} [\text{kV}]} + 0.0252/V_{RF} [\text{kV}]$ .

Another aspect of longitudinal evolution is shown in Figure 8 for 2000 turns for the smallest of the three amplitudes of the run shown in the middle (**E\_BM\_Z.RF.sxf**) case in Figure 3. Figure 9 differs only in that initial conditions have been adjusted to eliminate betatron oscillations.

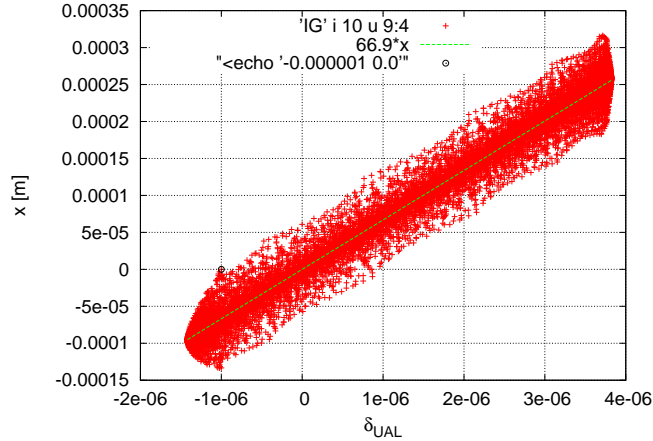


Figure 8: Starting at the black point, radial displacement  $x$  is plotted against fractional energy offset  $\delta_{UAL}$ . The straight line corresponding to  $D_{UAL} = 66.9$  m, as given by Eq. (12), can be seen to give an excellent fit to the data. The scatter of points can be ascribed to horizontal betatron oscillations.

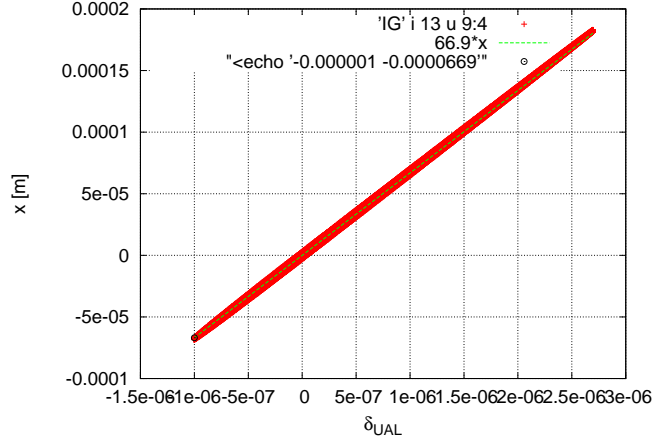


Figure 9: Same as Figure 8 except initial conditions have been assigned to minimize the initial horizontal betatron oscillation. So this is pure synchrotron oscillation, with radial position well fit by  $x = 66.9[m]\delta_{UAL}$ .

In Figure 10 only the initial horizontal slope is non-vanishing;  $x' = -0.0004$ . This is approximately the largest angle for which the particle will not be lost immediately on one of the electrodes which are situated at  $x = \pm 0.015$  m. The trajectory survives for the interval shown, but this particle will be lost eventually.

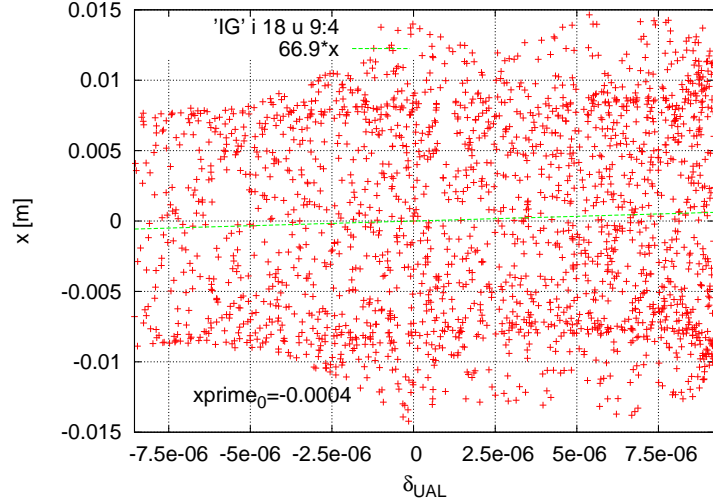


Figure 10: Large betatron amplitude, on-momentum, initially horizontal betatron motion in the `E_BM_M1.0.RF.sxf` lattice. Initial conditions are ( $x = 0.0, x' = -0.0004, \delta_{UAL} = 0$ ). The graph with opposite initial slope  $x' = 0.0004$  looks the same. With gap  $g$  being equal to 3 cm, this particle is just inside the physical acceptance for the 2000 turns shown. This particle wipes out eventually however; see Figure .

The top two graphs of Figure 11 shows the evolution of longitudinal position  $ct$  for small and large synchrotron oscillation amplitudes. This dependence is far from pure sinusoidal. An expanded view of the large amplitude motion is shown for a reduced time interval in the bottom figure. (But eye-ball comparison with the upper figure shows much the same distortion even for small synchrotron oscillation amplitude.)

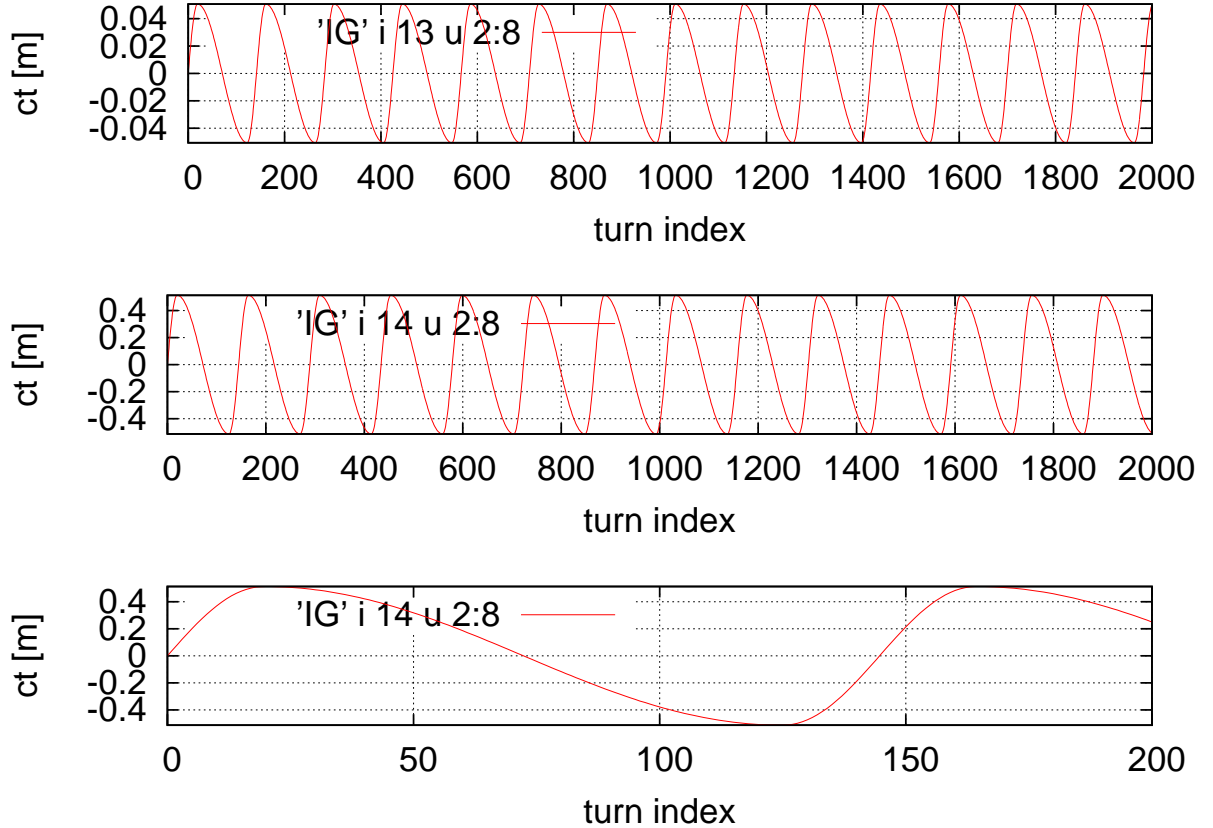


Figure 11: The upper graph plots longitudinal position  $ct$  vs. turn number for small amplitude synchroton oscillations. The tune  $Q_s$  is  $14.2/2000 = 0.0071$ . The middle graph plots the same quantities but for twenty times greater amplitude. The tune  $Q_s$  is  $13.2/2000 = 0.0066$ . The lower graph shows a bit more than one synchrotron period for the large amplitude case. Deviation from sinusoidal is pronounced, though not appreciably more than in the small amplitude case.

A possibly surprising aspect of the oscillation is illustrated by the bottom figure of Figure 11. The tracked particle executes longitudinal oscillations of amplitude  $\pm 0.5$  m. This graph can therefore be usefully compared with the outermost of the orbits shown in Figure 2. Both have a similarly large  $ct$ -ranges. The tracked particle starts side-by-side with the reference particle, but with too little speed ( $\delta_{UAL} = -10^{-5}$ ), as can be seen from Figure 2. Acting as if “above resonance” its shorter path length dominates is too-low speed, and it takes the tracked particle only 25 turns to get to the front of the bunch, as can be seen from Figure 11. But then it takes about 50 turns to get back level with the reference particle, and 50 turns more to get to the tail of the bunch. The time distortion in Figure 11 therefore corresponds to the up-down asymmetry in Figure 2.

Long term stability is investigated in Figure 12. For an intermediate case (third from the top) the beam blows up radially, and the blow up is fatal (in that the UAL code refuses to track transverse amplitudes greater than 1 m.) Particle survival for the large amplitude (bottom) case can be ascribed to sufficiently rapid passage through resonance for the particle to survive. In the actual pEDM apparatus this particle would, of course, not have survived since its maximum radial amplitude is 25 cm. This tracking was for lattice `E_BM_M1.0.RF.sxf` but the same plots for lattice `E_BM_Z.RF.sxf` were essentially the same. Both showed “resonant” particle blow up for too great oscillation amplitudes.

The upper two cases were stable for one million turns in a weekend long run. More quantitatively, the third plot, exhibited growth which, if interpreted as spurious, would correspond to a spurious growth lifetime of  $3 \times 10^6$  turns. The first 600 turns for the third plot in Figure 12. are shown in Figure 13. The

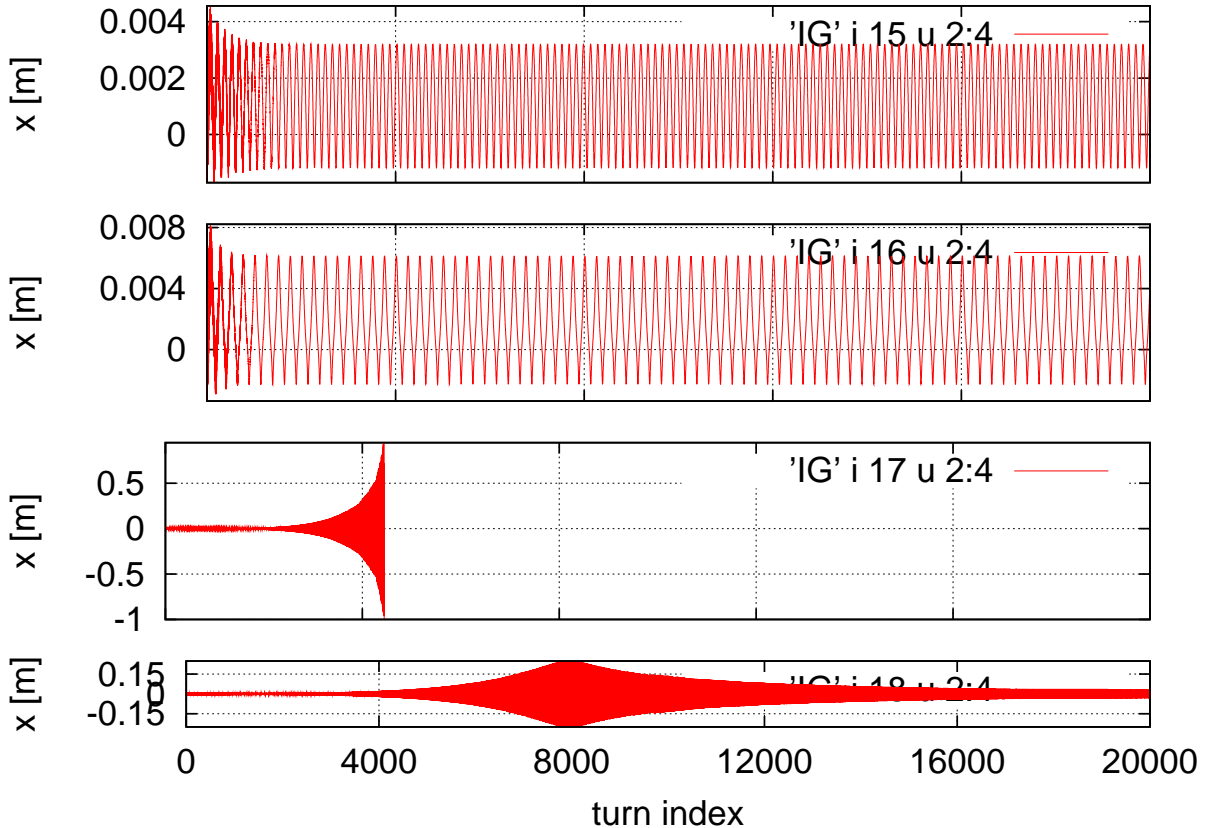


Figure 12: Tracking on-momentum particles with initial  $x'$  slopes of  $-0.00005$ ,  $-0.0001$ ,  $-0.0002$ , and  $-0.0004$  for 20,000 turns in the `E_BM_M1.0.RF.sxf` lattice. The default maximum amplitude at  $|x| = 1$  m terminates tracking in the  $x' = -0.0002$  case. Tracking in the `E_BM_Z.RF.sxf` lattice was essentially the same. Tracking for  $10^6$  turns showed nothing but boring extension for the upper three graphs, nor, (obviously) for the fourth. The fifth graph (call it “above resonance”) wanders non-periodically but remains bounded for at least  $10^5$  turns. In Figure 10 this case stays within the physical aperture for short times but, over long times it adiabatically increases to an amplitude that would cause it to wipe out on an electrode. But the particle would survive for electrode separation of 30 cm.

starting coordinates are  $(x, x', ct, UAL) = (0, 0.0001, 0, 0)$ . What we have been calling the betatron components of synchro- betatron oscillations damp out during this time (and never re-appear). Though the particle starts from  $x = 0$ , it ends up oscillating stably in the range 5–2 mm for at least a million turns therea

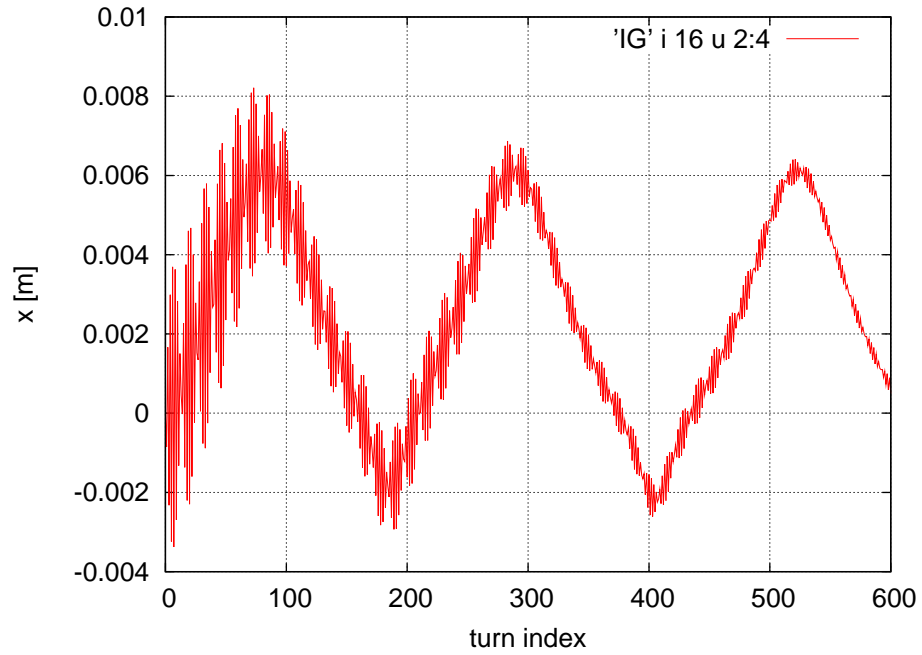


Figure 13: The first 600 turns for the second plot in Figure 12. The starting coordinates are  $(x, \dot{x}, ct, UAL) = (0, 0.0001, 0, 0)$ . What we have been calling the betatron component of synchro-betatron oscillation damps out during this time (and never reappears). Though the particle starts from  $x = 0$ , it ends up oscillating stably in the range 2–4 mm for at least a million turns thereafter. The fuzzy motion in this plot corresponds to the fuzzy motion in Figures 3.

## 6 Summary

### 6.1 Comments and (Tentative) Conclusions

With a few significant exceptions, the various plots exhibit behaviour much like what one sees in magnetic lattices. Various numerical comparisons of momentum-dependent ETEAPOT tracking results with analytic calculations and with results from the linearized transfer matrix model are listed in Table 2. With just one exception, there are no surprises here either. We consider the following points to be significant:

- We have found no significant differences in longitudinal dynamics among the three benchmark lattices (which have field index  $m = -1, 0, 1$ .) The discrete quadrupoles have been adjusted to give exactly the same vertical tunes and very nearly the same horizontal tunes. Apparently this constrains the longitudinal dynamics to be equivalent.
- There is essentially perfect agreement on the dispersion which is  $D_{\text{UAL}} = 66.9 \text{ m}$ . ( $D_{dp/p} = \beta_0 D_{\text{UAL}} = 40.1 \text{ m}$ .) Note, for example, Figure 9, which shows pure synchrotron oscillation with  $x[m] = 66.9 \delta_{\text{UAL}}$ .
- TEAPOT's determination of the small amplitude synchrotron tune is  $Q_s = 0.0071$ , which is significantly different from the “analytic” value  $Q_s = 0.0061$ . Noting that “analytic” and “correct” are not synonyms, clearly one or the other is wrong. Copied from the magnetic ring formalism, the analytic calculation assumes the absence of coupling between synchrotron and betatron oscillation, which is patently wrong. For reasons to be discussed we tend to believe the analytic result is oversimplified. (The linearized transfer matrix model determination does not provide an independent check of longitudinal motion other than the value of lattice dispersion.)
- What makes  $Q_s$  challenging is that it is hard to calculate the time of flight accurately. Apart from the fact that the fractional path length variations are minuscule, the change of velocity caused by change of potential has to be accounted for very accurately. Our calculation, based on analytic evaluation of the integral should, however be accurate and has been checked independently. For a preliminary version of this report the calculation of the time of flight using an analytic formula was made inaccurate in some cases by cancellation in the difference of large numbers. This numerical inaccuracy has been fixed for the present report.
- The analytic synchrotron oscillation theory, which is known to be reliable in the magnetic case, assumes there is no coupling between longitudinal and horizontal motion. In the electric case this is not the case, as can be seen numerically, for example, in Figure 13. We interpret the initial (for hundreds of turns) motion as sloshing between betatron and synchrotron oscillation.
- Previously we have feared that failure of symplecticity of the tracking code was responsible for the “damping” visible in the first several hundred turns, for example in Figure 12. But once this change has settled down there is negligible further attenuation, even for one million turns, which is how long the run was extended (taking two days, for twenty particles, on a laptop).
- The phase space has not been adequately investigated to obtain a horizontal admittance value. An order of magnitude estimate of the angular acceptance comes from  $|x'_{\max}| \approx \sqrt{\epsilon_{\text{admittance}}/\beta_x}$  or

$$\epsilon_{\text{admittance}} \approx \beta_x {x'_{\max}}^2 = 36 \times 0.0001^2 = 0.36 \times 10^{-6} \text{ m.} \quad (26)$$

This is something like three times smaller than has typically been assumed previously.

- The horizontal range explored by a particle launched with coordinates  $(x, x', ct, \delta_{\text{UAL}}) = (0.000001, 0, 0, 0)$  runs from  $-0.000001 < x < 0.000033 \text{ m}$ . The electric bending reduces the horizontal positional acceptance by a factor of three or so compared to the  $\pm 15 \text{ mm}$  imposed by the gap. Extrapolating

to the full acceptance, with gap  $g = 30$  mm, the horizontal acceptance is about  $\pm 4.5$  mm. Corresponding to Eq. (26), the horizontal admittance can be estimated from the horizontal position acceptance,

$$\epsilon_{\text{admittance}} \approx \frac{x_{\max}^2}{\beta_x} = \frac{0.0045^2}{36} = 0.56 \times 10^{-6} \text{ m.} \quad (27)$$

- There is a small angular correction term at bend edges that is not yet included in ETEAPOT. For normal incidence (which is nearly the case for all orbits) this angular, “refractive” deflection (caused by the change of potential) vanishes. This is why it has not been included. But, for safety, the effect of this term should be investigated.

## 6.2 Bug in the UAL/SXF Parser

(Obviously) synchrotron oscillations depend on the RF phase, which is read in via the `lag` entry in the SXF file. While checking the UAL/ETEAPOT time of flight code we discovered a bug in the pre-existing UAL/SXF parser. This bug causes the `lag` entry in the SXF file to be ignored, causing the `lag` to default to a default value of `lag=0`. This implicitly assumes that the average lattice dispersion is positive and is therefore the correct value for essentially all practical magnetic lattices.

The original SXF documentation does not specify the sign convention for the `lag` parameter. In the past it has apparently only been during investigation of passage through transition that the starting RF phase needs to be established carefully. Mimicking actual operations this phase has then been shifted impulsively during UAL simulations of longitudinal oscillations. But those simulations have used UAL/TIBETAN, which ignores the SXF `lag` parameter.

The policy for ETEAPOT development has been, and continues to be, to leave the SXF parsing (which has multiple implementations) completely unchanged. Instead, for the present report the default value of `lag=0.5` has been hard coded into ETEAPOT. This has produced the obviously stable oscillations exhibited in the present report.

## 6.3 Implications for Future ETEAPOT Simulations

The results of the present report strongly suggest that the magnitude of the lattice dispersion in the pEDM benchmark lattices is unacceptably large. This is discussed in detail in a separate report[6]. That report proposes a minimized-dispersion, combined function lattice that is strong-focusing horizontally and (as favored for the EDM measurement) weak-focusing vertically.

Of all the lattices that have been contemplated for the proton EDM experiment, this proposed lattice most nearly resembles the very first all-electric lattice, which was built at BNL for the very first alternating gradient proton accelerator[7]. (The very first functioning alternating gradient magnetic accelerator was an electron accelerator at Cornell.)

The field indices for the BNL AGS prototype were  $n = \pm 200$ , which are very much greater than our paltry values of  $m = -1, 0, 1$ . ( $m$  and  $n$  are similar exponents except for possible sign reversal and displacement by one or two units.)

In the ETEAPOT tracking formalism each orbit is made up of a sequence of perfect circles (within each slice of a bending element), with kinks at interspersed “virtual quadrupoles” to account for the actual field gradient, straight lines in the drift sections, and kinks at the true lattice quadrupoles (or other multipoles.) This approach is identical (for electric elements) to the bend-kick-bend formalism used by Etienne Forest[8] (for combined function bending magnets). This is the only known formalism for symplectic tracking through thick combined-function elements.

The ETEAPOT bend-kick-bend formalism has been especially appropriate for the weak-focusing benchmark lattices investigated in this report. Particle tracking has been unnecessarily accurate even with no artificial slicing of the bend elements. This has made it practical, for example, with meter long step sizes, to track for a million turns in a laptop computer.

The strong focusing elements in a minimum dispersion lattice will compromise this speed/accuracy trade-off seriously, especially for time of flight calculations, for which the phase slip error scales as the

square of the slice length. The strong focusing gradients in the minimum dispersion ring are about two orders of magnitude greater than the range of gradients tested in this report. This could make it necessary for the element slices to be about ten times smaller than we have been using.

But the phase slip error will tend to cancel in successive alternating gradient bends, the average dispersion will be unambiguously positive, and the gradient strengths will be comparable to those in rings (such as the AGS, the APS, or the Canadian Light Source) for which quite coarse slicing has been adequate. Nevertheless, simulations of the minimum dispersion EDM lattice may be as much as ten times slower than simulations in this report.

## References

- [1] J.D. Talman and R.M. Talman, *UAL/ETEAPOT Results (Augmented) for Proton EDM Benchmark Lattices*, BNL internal report, April 29, 2012
- [2] J.D. Talman and R.M. Talman, *UAL/ETEAPOT Proton EDM Benchmark Comparisons II: Transfer Matrices and Twiss Functions*, BNL internal report, August 30, 2012
- [3] D. Edwards and M. Syphers, *Longitudinal Motion*, p. 53 in *Handbook of Accelerator Physics and Engineering*, editors, A. Chao and M. Tigner, World Scientific, 2002
- [4] N. Malitsky, J. Talman, and R. Talman, *Appendix UALcode: Development of the UAL/ETEAPOT Code for the Proton EDM Experiment*, UAL/ETEAPOT documentation (frequently revised), August, 2012
- [5] Storage Ring EDM Collaboration, *A Proposal to Measure the Proton Electric Dipole Moment with  $10^{-29} e\text{-cm}$  Sensitivity*, especially Appendix 1. October, 2011
- [6] R. Talman, *Reduced Dispersion Proton EDM Storage Ring Lattices*, Internal Report, 12 December, 2012
- [7] M. Plotkin, *The Brookhaven Electron Analog, 1953-1957*, Brookhaven Internal Report, BNL-45058, 1991
- [8] E. Forest, *Beam Dynamics, A New Attitude and Framework*, Harwood Academic Publishers, 1998. See especially Section 12.2.3,